HHS Public Access

Author manuscript

Brain Stimul. Author manuscript; available in PMC 2020 July 01.

Published in final edited form as:

Brain Stimul. 2019 ; 12(4): 911–921. doi:10.1016/j.brs.2019.02.003.

The influence of respiration on brainstem and cardiovagal response to auricular vagus nerve stimulation: a multimodal ultrahigh-field (7T) fMRI study

Roberta Sclocco[1,2], **Ronald G. Garcia**[1,3], **Norman W. Kettner**[2], **Kylie Isenburg**[1], **Harrison P. Fisher**[1], **Catherine S. Hubbard**[1], **Ilknur Ay**[1], **Jonathan R. Polimeni**[1], **Jill Goldstein**[1,3,4], **Nikos Makris**[1,3], **Nicola Toschi**[1,5], **Riccardo Barbieri**[6,7], and **Vitaly Napadow**[1,2]

[1]Athinoula A. Martinos Center for Biomedical Imaging, Department of Radiology, Massachusetts General Hospital, Harvard Medical School, Charlestown, MA, USA

[2]Department of Radiology, Logan University, Chesterfield, MO, USA

[3]Department of Psychiatry, Massachusetts General Hospital, Harvard Medical School, Boston, MA, USA

[4]Department of Obstetrics and Gynecology, Massachusetts General Hospital, Harvard Medical School, Boston, MA, USA

[5]Department of Biomedicine and Prevention, University of Rome Tor Vergata, Rome, Italy

[6]Department of Electronics, Information and Bioengineering, Politecnico di Milano, Italy

[7]Department of Anesthesia, Critical Care and Pain Medicine, Massachusetts General Hospital, Harvard Medical School, Boston, MA, USA

Abstract

Background.—Brainstem-focused mechanisms supporting transcutaneous auricular VNS (taVNS) effects are not well understood, particularly in humans. We employed ultrahigh field (7T) fMRI and evaluated the influence of respiratory phase for optimal targeting, applying our respiratory-gated auricular vagal afferent nerve stimulation (RAVANS) technique.

Hypothesis.—We proposed that targeting of nucleus tractus solitarii (NTS) and cardiovagal modulation in response to taVNS stimuli would be enhanced when stimulation is delivered during a more receptive state, i.e. exhalation.

Corresponding Author: Roberta Sclocco, PhD, Athinoula A. Martinos Center for Biomedical Imaging, Department of Radiology, Massachusetts General Hospital, Harvard Medical School, 149 13th St, Charlestown, MA, 02129, roberta@nmr.mgh.harvard.edu.

Conflict of Interest

VN discloses consulting fees from Glaxo Smith Kline and Cala Health, for whom he serves on the scientific advisory board; JG discloses consulting for Cala Health and serving on the scientific advisory board. All other authors have no known conflicts of interest associated with this publication.

Methods.—Brainstem fMRI response to auricular taVNS (cymba conchae) was assessed for stimulation delivered during exhalation (eRAVANS) or inhalation (iRAVANS), while exhalation-gated stimulation over the greater auricular nerve (GANctrl, i.e. earlobe) was included as control. Furthermore, we evaluated cardiovagal response to stimulation by calculating instantaneous HF-HRV from cardiac data recorded during fMRI.

Results.—Our findings demonstrated that eRAVANS evoked fMRI signal increase in ipsilateral pontomedullary junction in a cluster including purported NTS. Brainstem response to GANctrl localized a partially-overlapping cluster, more ventrolateral, consistent with spinal trigeminal nucleus. A region-of-interest analysis also found eRAVANS activation in monoaminergic source nuclei including locus coeruleus (LC, noradrenergic) and both dorsal and median raphe (serotonergic) nuclei. Response to eRAVANS was significantly greater than iRAVANS for all nuclei, and greater than GANctrl in LC and raphe nuclei. Furthermore, eRAVANS, but not iRAVANS, enhanced cardiovagal modulation, confirming enhanced eRAVANS response on both central and peripheral neurophysiological levels.

Conclusion.—7T fMRI localized brainstem response to taVNS, linked such response with autonomic outflow, and demonstrated that taVNS applied during exhalation enhanced NTS targeting.

Introduction

The vagus nerve is critically involved in autonomic regulation of several visceral organs, including the heart, lungs, pancreas, and portions of the gastrointestinal tract. In the last couple of decades, the cervical bundle of the vagus (Cranial Nerve X) has been a target for vagus nerve stimulation (VNS) therapy. However, given the invasiveness and cost of the surgical VNS procedure, its therapeutic application has been mostly limited to brain-based targets: drug-resistant epilepsy and major depression (Ben-Menachem et al. 1994; Handforth et al. 1998; Sackeim et al. 2001; Nemeroff et al. 2006). More recently, two main non-invasive approaches (nVNS) have emerged, one targeting the cervical vagus nerve in the neck (transcutaneous cervical VNS, tcVNS), the other targeting the auricular branch of the vagus nerve (ABVN; transcutaneous auricular VNS, taVNS). The latter, taVNS, has been employed for patients suffering from various disorders including epilepsy (Ventureyra 2000), chronic tinnitus (Lehtimaki et al. 2013; Kreuzer et al. 2014), depression (Rong et al. 2012; Hein et al. 2013), pain (Napadow et al. 2012; Laqua et al. 2014; Garcia et al. 2017; Janner et al. 2018), migraine (Straube et al. 2015; Garcia et al. 2017), as well as in cardiovascular modulation (Clancy et al. 2014; Antonino et al. 2017; Badran et al. 2018b). While clinical taVNS applications have been widely noted in the literature, the physiological mechanisms supporting such clinical effects are not well understood, particularly in humans.

The primary synaptic target of afference over the vagus nerve is the nucleus tractus solitarii (NTS), located in the dorsal medulla. This elongated nucleus extends rostroventrally from the ponto-medullary junction to just below the obex, where it merges with the contralateral column. The NTS transfers information to premotor parasympathetic nuclei including nucleus ambiguus (NAmb) and dorsal motor nucleus of the vagus. In fact, taVNS has also demonstrated robust modulation of autonomic outflow using heart rate variability (HRV) and other measures (Clancy et al. 2014; Antonino et al. 2017; Ylikoski et al. 2017).

Moreover, ascending projections from NTS transfer afference to higher monoamine neurotransmitter source nuclei such as locus coeruleus (LC, noradrenergic) and raphe (serotonergic) nuclei in the pons and midbrain (Loewy et al. 1978; Norgren 1978; Van Bockstaele et al. 1999; Saper et al. 2015), which may also impact autonomic outflow via feedback loops, as well as modulating higher brain function by recruiting these diffusely projecting neurotransmitter systems.

Importantly, NTS activity is known to be modulated by respiration, both through bottom-up afference from pulmonary stretch receptors and aortic baroreceptors, and via top-down influence from ventral respiratory group nuclei in the medulla. Specifically, NTS receives inhibitory influence during inhalation, and facilitatory influence during exhalation (Miyazaki et al. 1998; Miyazaki et al. 1999; Baekey et al. 2010). Therefore, our group has proposed that NTS targeting by taVNS can be enhanced by gating stimulation to the exhalation phase of the respiratory cycle via respiration-gated auricular vagal afferent nerve stimulation (RAVANS) (Napadow et al. 2012; Garcia et al. 2017). In this context, exhalation-gated RAVANS (eRAVANS) produced promising antinociceptive effects compared to non-vagal auricular stimulation in chronic pain patients (Napadow et al. 2012), and modulated trigeminosensory brain response in LC and raphe nuclei in migraine patients (Garcia et al. 2017). Thus, targeting NTS might be optimized by delivering stimulation during a more receptive state (i.e. exhalation).

Our study investigated evoked brain response to taVNS stimuli, which may support the neurophysiological and clinical effects noted above. While multiple functional magnetic resonance imaging (fMRI) studies have aimed at evaluating brain response to taVNS in humans (Kraus et al. 2007; Dietrich et al. 2008; Kraus et al. 2013; Frangos et al. 2015; Garcia et al. 2017; Usichenko et al. 2017; Yakunina et al. 2017; Badran et al. 2018a), the challenges posed to brainstem functional imaging by physiological noise and the small cross-sectional area of many brainstem nuclei has limited signal-to-noise ratio (SNR) in such nuclei and hampered precise characterization of taVNS-related responses. Advances in ultrahigh-field MRI (UHF, 7T and higher) have proven instrumental in overcoming some of these SNR limitations, significantly expanding the field of brainstem imaging (Sclocco et al. 2018). Our UHF fMRI approach sought to better localize evoked brainstem response to taVNS using focused cardiovascular noise removal and flexible hemodynamic response function setting, allowing us to reliably assess the influence of respiration-gating. Additionally, we evaluated concurrent instantaneous HRV response to taVNS using a statistical model-based spectral approach previously developed by our group (Barbieri et al. 2005) to investigate cardiovagal stimulus-evoked response, and tested the association of the autonomic outflow with brainstem fMRI response. To our knowledge, this is the first study applying UHF fMRI to identify specific brainstem region responses to taVNS and link the response with autonomic outflow.

Methods

Subjects

Sixteen (16) healthy adult subjects (9 female, age: 27.0 ± 6.6 years, mean ± SD) were enrolled. All study procedures were approved by the local Institutional Review Board, and

written informed consent was provided by all subjects. Subjects were excluded from participation in case of major neurological or other medical disorders that would interfere with study procedures or confound results (e.g. conditions altering blood flow), a history of seizure or significant head trauma, a history of Axis I psychiatric diagnosis, as well as any contraindication for MRI. Prior to the MRI scanning, participants were familiarized with the stimulation and calibration procedure. Specifically, they were instructed to rate the intensity of the stimulation using a numeric rating scale (NRS) ranging from 0 ("no sensation") to 10 ("pain threshold"), and to aim for a "moderately strong, but not painful sensation", corresponding to a target score of 4 to 5 on the 0-10 scale. Subjects were told they would experience the stimulation intermittently during the imaging session. Subjects were not told, and were unaware of (by qualitative debriefing following the MRI scan session), respiration gating for any stimulation procedure during this study.

Experimental protocol

Each subject underwent a single visit MRI scan session consisting of four 8-minute duration fMRI scan runs, including a passive control scan, two active stimulation scans, and an active control scan run (Figure 1). Specifically, after an initial fMRI scan run during which sham stimulation was provided (i.e., electrode placed within cymba conchae, but no electrical current passed), subjects experienced three stimulation runs. For these scan runs, taVNS stimulation was gated either to the exhalation or inhalation phase of the respiratory cycle (eRAVANS, iRAVANS), while a third fMRI run included a control with exhalation-gated stimulation of the greater auricular nerve innervated earlobe location (GANctrl)). The sham stimulation fMRI run was performed first in order to maintain blinding for active versus inactive stimulation, and the order of the three active stimulation runs was counterbalanced across subjects. Stimulus intensity (current amplitude, mA) was set by percept-matching across subjects (target score of 4 to 5 on the 0-10 NRS reported above) just prior to each scan run, and intensity ratings were assessed again at the end of each run.

Stimulation

Stimuli consisted of biphasic rectangular pulse trains with 450 μs pulse width and a duration of 1 s, delivered at 25 Hz, and provided by a current-constant Model S88x stimulator with stimulus isolation unit (Grass Instruments, Astro-Med, Inc, West Warwick, RI, USA). RAVANS taVNS was delivered via custom-built, ergonomically-shaped MR-compatible electrodes (Bionik Medical Devices, Bucaramanga, Colombia) placed within the left cymba conchae of the ear (Figure 1). A second set of electrodes was secured to the left earlobe prior to scanning, and used to deliver control-location stimulation (GANctrl). The respiratory gating was implemented by measuring respiration through a custom-built pneumatic belt placed around the subjects' lower thorax. Low-compliance tubing connected the belt to a pressure transducer (PX138-0.3D5V, Omegadyne, Inc., Sunbury, OH, USA), and the voltage signal reflecting respiratory volume was acquired by a laptop-controlled device (National Instruments USB DAQCard 6009, 14-bit i/o, with LabView 7.0 data acquisition software). In-house developed LabView© code was used to detect end-inhalation and end-exhalation in real-time, based on an adaptive threshold detection algorithm, and a TTL signal was sent to a miniature high-frequency relay (G6Z-1P-DC5, Omron Electronics Components, Shaumburg, IL, USA), thereby controlling the onset and offset of stimulation. A brief 0.8 s delay was

introduced between the end-inhalation timestamp and stimulus onset for exhalation-gated stimulation, in order to ensure delivery during the exhalation phase. As the inhalation phase is shorter than the exhalation phase, a nominal 0.1 s delay was used for inhalation-gated stimulation. Potential differences in stimulation parameters and ratings across conditions were explored using repeated measures ANOVAs implemented in Matlab (R2016b, The MathWorks, Natick, MA, USA). Sham taVNS stimulation was provided during a separate fMRI scan run by disconnecting the stimulation electrode from the current source, while maintaining the identical auricular electrode placement on the subject.

MRI and physiological data collection

Blood oxygenation level-dependent (BOLD) fMRI data were collected on a Siemens 7 T whole-body scanner (Siemens Healthineers, Erlangen, Germany) using a custom-built 32-channel receive array and birdcage transmit coil. Functional MRI data were acquired with gradient-echo single-shot echo-planar imaging (EPI) using a Simultaneous Multi-Slice acquisition with multi-band factor 2 and the following parameters: 1.2 mm isotropic voxel size (field of view = 192 χ 192 mm^2), 38 coronal slices centered on the brainstem and tilted parallel to the dorsal border of the brainstem using a mid-sagittal localizer, repetition time (TR) = 0.99 s, echo time (TE) = 23 ms, flip angle = 58° band width = 1562 Hz pix^{-1}, echo spacing = 0.76 ms, using R = 4 in-plane (generalized autocalibrating partially parallel acquisitions (GRAPPA)) acceleration and a robust autocalibration scan (Polimeni et al. 2016). For each fMRI scan run, 500 time-series measurements were acquired. To aid co-registration, a T2*-weighted anatomical reference dataset was also acquired using the same EPI pulse sequence, modified to provide whole-brain coverage but retaining the orientation and shimming volume of the partial-brain data (126 coronal slices, TR = 3.29 s). For both the functional runs and the anatomical reference scan, an additional volume was collected having opposite phase encoding, which was used to estimate and correct susceptibility-induced distortion (topup, FSL). Concurrent with MRI scanning, electrocardiogram (ECG) and respiration signals were continuously collected at 500 Hz using an MRI-compatible, noninvasive BIOPAC MP150 system (BIOPAC Systems, Goleta, CA) and a laptop equipped with AcqKnowledge acquisition software (BIOPAC Systems).

MRI data preprocessing

For fMRI, data preprocessing was performed using a combination of the Oxford Centre for Functional MRI of the Brain (FMRIB) Software Library (FSL; v. 5.0.7), the Analysis of Functional NeuroImages (AFNI), and in-house bash scripts. The fMRI images were corrected for cardiorespiratory noise (RETROICOR), slice timing (using a custom script accounting for the Simultaneous Multi-Slice acquisition of the dataset), susceptibility-induced distortion (estimated using topup, FSL), and head motion (MCFLIRT, FSL). Following these preprocessing steps, the whole-brain volume, sharing the same orientation and distortion as the partial-brain fMRI runs, was normalized to a T2-weighted MNI template (ICBM 2009a Nonlinear Asymmetric template (Fonov et al. 2011) using linear and nonlinear transformations (FSL FLIRT and FNIRT, respectively). The high spatial resolution (1.2 mm isotropic voxels) and strong tissue contrast afforded by ultrahigh-field imaging allowed us to avoid the additional step of functional-to-anatomical co-registration, thus reducing possible misalignments due to variable susceptibility-induced distortion across

sequences. A brainstem mask, defined in the ICBM152 MNI space by thresholding gray and white matter tissue maps at a tissue probability of 0.9 (as in prior studies (Beissner et al. 2014; Moher Alsady et al. 2016; Garcia et al. 2017)), was then transformed into individual functional spaces by inverting the estimated transform matrices (Figure 2A). This mask was used to select and retain only brainstem fMRI voxels from the original dataset, in order to remove spatial smoothing-induced contamination of parenchymal voxels with fMRI signal from vascular and other non-parenchymal structures surrounding the brainstem such as cerebrospinal fluid (CSF), known to be heavily affected by physiological noise. Following this masking step, minimal spatial smoothing with a Gaussian smoothing kernel (full width at half maximum (FWHM) = 2 mm) was applied to the BOLD fMRI data.

MRI data analysis

For auricular stimulus fMRI scan runs, first-level General Linear Model (GLM) analyses of brainstem fMRI data were carried out using an event-related design and the fMRI Expert Analysis Tool (FEAT v6.00, FSL). Because the hemodynamic impulse response may deviate from the canonical hemodynamic impulse response function due to our target brainstem location, for each fMRI scan run, stimulation timings were convolved with a set of three basis functions chosen through FMRIB's Linear Optimal Basis Set (FLOBS, FSL) algorithm, designed to provide flexibility in the shape of the hemodynamic response function. To account for the potential for the brainstem response to be faster than the canonical response (Lewis et al. 2018), the FLOBS basis set was designed to span hemodynamic delays between 1 and 8 s. Brainstem response to sham stimulation (exhalation-gated sham, eSham, and inhalation-gated sham, iSham) was assessed to control for any generalized fMRI signal response to neural or non-neural respiratory-based modulation. For both eSham and iSham, we used the respiratory signal collected during the corresponding fMRI scan run to define sham stimulus events for event-related fMRI analyses, thereby controlling for respiratory cycle influence on the brainstem fMRI signal. To further control for cardiac-driven contamination of the brainstem fMRI signal, instantaneous heart rate, as estimated through the point-process algorithm (see below), was convolved with the previously-reported cardiac response function (Chang et al. 2009) and included in the design matrix as a regressor of no interest.

Following this first level analysis, individual parameter estimates (PEs) derived from the three FLOBS basis functions were combined in a signed root mean square (RMS) summary statistic (Calhoun et al. 2004). The resulting distribution of this summary statistic is highly non-Gaussian, therefore all group-level analyses were carried out using nonparametric permutation analysis (5000 randomizations; randomise, FSL). Individual summary statistics were then transformed to MNI space and concatenated for each condition, and brainstem responses were evaluated by comparing each active stimulation condition with the appropriate sham stimulation condition, using paired nonparametric randomization tests: eRAVANS–eSham, iRAVANS–iSham, GANctrl–eSham. Two sets of analyses were performed. The first analysis was aimed at evaluating ipsilateral dorsal medullary response (site of primary synapse for afference from the auricle, e.g. NTS, spinal trigeminal nucleus (SpV)). We used a small-volume approach in which a search volume was defined in the dorsal medulla ipsilateral to the stimulation site, which was defined by a caudal limit set by

the fMRI data field-of-view, a rostral limit set by the pontomedullary junction, and a ventral limit set by the reticular formation (Figure 2C). Given to the limited signal-to-noise ratio (SNR) typical for brainstem responses (Brooks et al. 2013; Beissner et al. 2014; Sclocco et al. 2018), significance within this small-volume search space was set at uncorrected $p < 0.05$. Additionally, in the Supplementary Material, we also display unmasked (whole-brainstem) results thresholded at uncorrected $p < 0.05$ (Supplementary Figure S1). Significant fMRI clusters were localized with the aid of two brainstem atlases, Duvernoy's Atlas of the Human Brain Stem and Cerebellum (Naidich et al. 2009) and Olszewski and Baxter's Cytoarchitecture of the Human Brainstem (Olszewski et al. 1954). In a second analysis, the same contrasts were estimated in the entire brainstem volume, and a region of interest (ROI) approach was used with MNI-space masks for specific neurotransmitter nuclei hypothesized to be modulated by taVNS. These included bilateral locus coeruleus (LC), and dorsal and median raphe nuclei (DR, MR) (Figure 2D), identified from results of previously published T1 turbo spin echo MRI (Keren et al. 2009) and [^{11}C]DASB positron emission tomography (PET) binding (Beliveau et al. 2015) neuroimaging studies specifically designed to identify these nuclei. For each ROI, an outcome metric was calculated with an Extent/Activation Index (EAI), defined as follows:

$$EAI_{ROI} = \overline{sumstat}_{p<0.05} \times \frac{\#\ voxels_{p<0.05}}{\#\ ROI\ voxels} \times 100$$

The EAI index weighs the average value of the FLOBS summary statistics from significant ($p<0.05$) voxels within each ROI by a multiplicative factor quantifying the percentage of overlapping voxels with respect to the total number of voxels in the ROI, thus preventing a very significant, but spatially limited (i.e., a few voxels) activation from driving the outcome metric. The multiplicative factor is calculated at the group level for each condition (eRAVANS–eSham, iRAVANS–iSham, GANctrl–eSham), and then used to weigh the average value of the summary statistics over the ROI, extracted at the single subject level. The EAI indices for the different ROIs were then compared across conditions using paired t-tests. Significance was set at $p < 0.05$, Bonferroni-corrected for multiple comparisons.

Use of high-resolution anatomical underlay

In order to aid visualization and anatomical localization, functional activation results were displayed over an *ex vivo*, high resolution (0.2 mm isotropic) brainstem dataset (B_0 image from DTI acquisition) generously provided by the lab of Dr. Alan Johnson (Calabrese et al. 2015). Accurate co-registration between this *ex vivo* brainstem volume and MNI space (which contained our fMRI maps) was performed using the Advanced Normalization Tools (ANTs) Toolbox (Avants et al. 2014) and 3D Slicer (www.slicer.org). Specifically, manual landmark-based affine registration was first completed using the first step of our previously published ABC brainstem co-registration method (Napadow et al. 2006). Subsequently, 3D Slicer was used to generate a brainstem mask on a 0.5 mm resolution MNI152 T1 template, which was dilated to include high-contrast boundaries and used to select the brainstem volume. The ANTs Toolbox was then used to perform a generic affine registration followed by Symmetric Normalization deformation using the default parameters and mutual information as similarity metric. Quality of co-registration was excellent for the medullary

and pontine regions reported in our study (Figure 2B, Supplementary Figure S2). The estimated transformation matrices were then used to transform fMRI group level maps from MNI space to the high-resolution brainstem space for visualization.

Cardiovagal response analysis using instantaneous HF-HRV

For cardiovagal analysis, ECG segments relative to each run were first annotated to identify the R-wave peak using an automated in-house algorithm followed by manual inspection. Similar to our prior studies, a point-process method was used to develop local likelihood HR estimation from the R-to-R interval series (Barbieri et al. 2005).

Briefly, each series is modeled by an inverse Gaussian probability function describing the time interval before each successive heartbeat. The mean of this probability function is modeled using a linear autoregressive model of order k, thus characterizing the dependence of the current time interval on the last k beat-to-beat intervals. From this set of autoregressive coefficients, instantaneous spectral measures of heart rate variability (HRV) were integrated in canonical frequency bands, thus computing the power within the high-frequency (HF-HRV, 0.15–0.40 Hz) range (Camm et al. 1996). As in our previous studies (Napadow et al. 2008; Sclocco et al. 2014; Sclocco et al. 2016), the instantaneous HF-HRV index was chosen as a metric for parasympathetic (cardiovagal) activity, in order to estimate stimulus-evoked cardiovagal response. This instantaneous spectral approach allowed for assessment of peri-stimulus HF-HRV response to stimulation, not allowed by standard, non-time-varying frequency space HRV index estimation.

The instantaneous HF-HRV power time series were then segmented into individual epochs starting 0.5 s before each 1-second stimulation train, extending 2 s after the end of each stimulation (3.5 s epoch total duration). For analysis, pre-stimulation samples were used as a baseline, and percent HF-HRV variations were calculated for each event and averaged over the scan run and across subjects, in order to estimate the stimulus-evoked cardiovagal modulation response. Moreover, linear regression analysis evaluated any correlation between cardiovagal response and brainstem response for the ROIs defined above, using individual summary statistic values (significant at $p<0.05$).

Results

All subjects tolerated the stimulation and completed the experimental sessions without adverse events. Stimulation characteristics across different conditions demonstrated no significant differences for stimulation current (F-score = 0.45, p-value = 0.64) or ratings of intensity (F-score = 0.06, p-value = 0.56) (Table I). Individual current sensitivity across conditions was consistent – that is, subjects requiring higher stimulation currents in one stimulation run, also required higher currents in the others – as measured by a significant intraclass correlation coefficient (ICC = 0.75, p-value < 0.01). Trending, but non-significant differences, were noted for number of stimuli delivered (repeated measures ANOVA F-score = 2.58, p-value = 0.07) and inter-stimulus interval between stimuli (F-score = 2.67, p-value = 0.06), with slightly more stimuli and shorter ISI for iRAVANS on average. Furthermore, while order was randomized, no significant correlations were found between the order of

active conditions (eRAVANS, iRAVANS, GANctrl) and stimulation characteristics or subjects' ratings.

Brainstem medullary response for each active condition was visualized over the high-resolution *ex vivo* dataset for localization (Figure 3). Each active stimulation map was normalized by exhalation- or inhalation-gated sham stimulation fMRI response map, and the eRAVANS – eSham (hereinafter, eRAVANS') contrast showed a positive contrast (p-value < 0.05, uncorrected within the small-volume mask) in an elongated cluster extending rostro-ventrally within the rostromedial to rostrolateral medulla. Based on brainstem atlases (Olszewski et al. 1954; Naidich et al. 2009), this cluster encompassed purported rostral NTS, NAmb and the dorsoventral portion of the olivary nucleus. No significant responses were found for the iRAVANS – iSham (iRAVANS') contrast. While there were no significant differences found when directly contrasting eRAVANS and GANctrl, interesting offsets in localization were found for the normalized eRAVANS and GANctrl responses (red/yellow and green, respectively), as well as their overlap (blue) (Figure 3). Results demonstrated that the GANctrl cluster had a more rostrolateral location consistent with SpV, while the eRAVANS cluster was more dorsomedial and extended more caudally, consistent with the known anatomical morphology of NTS. When formally comparing eRAVANS and iRAVANS (i.e. eRAVANS' – iRAVANS', Figure 4), a similar elongated cluster was revealed, and included rostral NTS and NAmb. The GANctrl – eSham (GANctrl') difference map showed a cluster located on the rostral edge of the search volume, and included purported dorsoventral olive / reticular formation, as well as SpV. The same analyses were repeated adding individual current levels as a regressor of no interest in the group design matrix, in order to control for the different current intensities due to our percept-matched approach to calibration. The resulting maps were nearly identical to those shown in Figures 3 and 4, suggesting that current amplitude, while highly variable across subjects, did not significantly influence group differences.

In ROI analyses, significantly higher EAI values ($p < 0.05$, Bonferroni-corrected) were found for eRAVANS' compared to both iRAVANS' and GANctrl' in right LC (eRAVANS': 969.7 ± 1299.9 a.u., mean ± SD; iRAVANS': 99.9 ± 302.9 a.u.; GANctrl': 114.8 ± 238.9 a.u.), DR nucleus (eRAVANS': 66.2 ± 100.8 a.u.; iRAVANS': 0 a.u.; GANctrl': 0 a.u.) and MR nucleus (eRAVANS': 867.7 ± 1184.9 a.u.; iRAVANS': 161.0 ± 402.6 a.u.; GANctrl': 0 a.u.) (Figure 5).

Cardiovagal analysis found that compared to pre-stimulation baseline for each stimulus event, the HF-HRV stimulus-evoked response was significantly increased during the stimulation period for both eRAVANS' and GANctrl', while no significant deviation from baseline was found for iRAVANS' (Figure 6A). Furthermore, cardiovagal response to eRAVANS showed increased values up to 2 s after the beginning of the stimulation period and the subjects' average HF-HRV change score in this 2 s post-eRAVANS onset window was correlated with fMRI response (FLOBS summary statistic) in the MR nucleus (Pearson's $r = 0.51$, p-value = 0.04; Figure 6B). Thus, subjects with greater response in this serotonergic source nucleus also demonstrated greater cardiovagal modulation.

Discussion

The brainstem circuitry activated and modulated by taVNS has been challenging to evaluate in humans due to neuroimaging limits on spatiotemporal resolution and the strong physiological noise inherent to fMRI found within this important brain region (Sclocco et al. 2018). Our study characterized brainstem response to taVNS applied to the cymba conchae of the left ear by exploiting the increased spatiotemporal resolution provided by ultrahigh-field (7T) fMRI. We explored the influence of respiratory phase on stimulation outcome by delivering stimulation during exhalation (eRAVANS) or inhalation (iRAVANS), and employed greater auricular nerve stimulation (GANctrl, electrodes placed on the earlobe) as a sensory control. Furthermore, we evaluated cardiovagal response (instantaneous HF-HRV) to stimulation, using cardiac data recorded concurrently with fMRI. For eRAVANS, we found stimulus-evoked activation in an ipsilateral pontomedullary region consistent with NTS, and activation was significantly more robust compared to inhalation-gated taVNS. Moreover, eRAVANS activation in this region was partially overlapping but spatially offset from the ipsilateral pontomedullary region activated by GANctrl stimulation, which was consistent with the location of the SpV nucleus.

Additionally, an ROI analysis found greater activation for eRAVANS, compared to both iRAVANS and GANctrl, in important monoamine neurotransmitter source nuclei such as locus coeruleus (LC, noradrenergic) and median and dorsal raphe (MR, DR, serotonergic) nuclei. Furthermore, eRAVANS also increased HF-HRV, and greater increase in HF-HRV was associated with greater activation in the pontine median raphe nucleus. This suggests that this serotonergic source nucleus may play a role in the feedback regulatory loop by which auricular taVNS upregulates cardiovagal outflow. Our results localize taVNS targeting in the human brainstem, and demonstrate that exhalation-gated stimulation can enhance NTS targeting and cardiovagal modulation compared with inhalation-gated and sham control.

Results demonstrated enhanced ipsilateral NTS response for eRAVANS compared to iRAVANS. This nucleus is known to contain the primary synapse for ABVN afference into the brainstem, and a gateway by which ABVN stimulation can modulate higher brainstem and even cortical function in the brain. Thus, NTS activation could serve as a viable target for future taVNS optimization across different parameter spaces (e.g. frequency, pulse width, etc.). We proposed that a non-obvious parameter space includes respiratory phase, and attribute enhanced NTS activation during exhalation to both bottom-up and top-down influence. Firstly, the NTS receives afference during inhalation over the main trunk of the vagus from pulmonary stretch receptors and aortic baroreceptors (Piepoli et al. 1997), potentially competing with any ABVN afference to NTS. The NTS is also known to receive inhibitory inputs from ventral respiratory group (VRG) nuclei in the medulla during inhalation and facilitation during exhalation (Miyazaki et al. 1998; Miyazaki et al. 1999). Ultimately, we suggest that both of these influences set up a more receptive state for ABVN input during exhalation.

We also found stimulus-evoked activation in other medullary nuclei, consistent with SpV and NAmb, with greater activation for eRAVANS compared to iRAVANS. SpV is

ventrolateral to NTS in the dorsal pontomedullary junction and is also known to receive afferent input over ABVN fibers (Nomura et al. 1984; Kiyokawa et al. 2014). Moreover, GANctrl stimulation also produced robust activation in ipsilateral medulla, in a cluster consistent with SpV, and ventrolateral to the NTS cluster activated by eRAVANS. The greater auricular nerve is a superficial cutaneous branch of the cervical plexus, composed of branches of spinal nerves C2 and C3, whose afferent fibers terminate in the cuneate and SpV nuclei in the medulla (Liu et al. 1988). Thus, our GANctrl stimulation was not physiologically inert, and future studies evaluating clinical effects of taVNS should use caution in applying earlobe stimulation as a placebo control. In fact, its use has been recently debated in a series of commentaries (Keute et al. 2018; Rangon 2018), although no consensus has been reached regarding a suitable alternative.

On the other hand, NAmb is a smaller-diameter elongated structure and the main premotor nucleus for vagal outflow to the heart. Respiratory phase may also be an important variable for stimulus-evoked response in this nucleus, as breathing is known to introduce rhythmical oscillations in cardiovagal physiology. During each respiratory cycle, heart rate decreases during exhalation and increases during inhalation, matching pulmonary blood flow to lung inflation and maintaining an appropriate oxygen diffusion gradient (Wehrwein et al. 2013). This “respiratory sinus arrhythmia” (RSA) occurs by modulation of premotor cardiovagal neurons (e.g. NAmb) by diverse mechanisms, including afference (via NTS) from the lungs, and thoracic baroreceptors, as well as direct input from medullary respiratory neurons (Dergacheva et al. 2010; Wehrwein et al. 2013; Zoccal et al. 2014). In fact, NTS neurons play a direct role in coordinating RSA (Zoccal et al. 2014), as activation of excitatory 2nd-order NTS neurons increases premotor cardiovagal neuron firing rate and inhibits premotor sympathetic neurons (Spyer 1981; Schreihofer et al. 2003). In contrast, during inhalation, activity of ventral respiratory group medullary neurons leads to inhibitory GABAergic and glycinergic synaptic transmission to premotor cardiovagal neurons (Gilbey et al. 1984; Neff et al. 2003). Our results show that ABVN input during exhalation also facilitates NAmb activation.

Interestingly, eRAVANS evoked activation within important noradrenergic (LC) and serotonergic (MR, DR) brainstem source nuclei. Evoked fMRI response was significantly greater compared to both iRAVANS and GANctrl, suggesting that more robust NTS targeting also translates to greater activation of these higher pontine/midbrain nuclei. In fact, both noradrenergic and serotonergic regulation has been posited to be a mechanism supporting taVNS clinical outcomes (Yuan et al. 2015). LC, a columnar structure located bilaterally in the dorsal pons, contains the highest number of noradrenergic neurons in the brain, and is the origin of extensive and diffuse descending and ascending projections. The LC-noradrenaline system has been implicated in the modulation of a variety of higher cognitive and affective functions, including enhancement of arousal state (Amatruda et al. 1975; Aston-Jones et al. 1981), execution of adaptive behavioral responses (Aston-Jones et al. 2005), and memory consolidation and retrieval (Sara 2009; Jacobs et al. 2015).

The raphe nuclei, on the other hand, are the largest collection of serotonergic neurons in the brain, and are clustered throughout the midline, extending from the medulla to the midbrain. The principal ascending fibers originate from MR and DR, located in the midbrain/pons and

midbrain respectively, and target other midbrain nuclei, as well as subcortical and cortical structures (Vertes et al. 2008; Dorocic et al. 2014). Serotonin is a monoaminergic neuromodulator involved in a broad range of cognitive/affective functions including emotion (Meneses et al. 2012), reward (Liu et al. 2014), pain (Wang et al. 1994), sleep (Monti 2010), and motor activity (Di Matteo et al. 2008). In sum, LC and raphe activation likely follows stimulation-evoked response in NTS, which is known from animal studies to project to peri-LC dendrites (Van Bockstaele et al. 1999) and to midbrain raphe nuclei (Jacobs et al. 1992). Furthermore, DR and MR nuclei receive substantial afferents from the parabrachial nucleus (Saper et al. 1980; Lee et al. 2003), which is also a target of NTS ascending fibers (Saper et al. 2015), and may modulate raphe nuclei activity by this indirect pathway.

Interestingly, our previous RAVANS fMRI study showed that following RAVANS there was increased LC and MR response to trigeminal sensory afference (forehead airpuff stimulation) in migraineurs (Garcia et al. 2017), consistent with the hypothesis that serotonergic/noradrenergic regulation of abnormal trigeminal somatosensory processing supports the therapeutic effects of taVNS in migraine (Straube et al. 2015). Our ultrahigh-field (7T) fMRI results demonstrated that eRAVANS also produces stimulus-evoked response in LC and raphe nuclei, more closely linking taVNS with serotonergic and noradrenergic regulation.

Additionally, cardiovagal modulation, as measured by instantaneous HF-HRV power, showed stimulus-evoked increase during eRAVANS and GANctrl stimulations, with more sustained response (up to 2 s after stimulation onset) for eRAVANS. No significant stimulus-evoked HF-HRV response was found for iRAVANS. These results are consistent with the brain imaging findings, confirming a lack of effect of iRAVANS at both central and peripheral neurophysiological levels. Interestingly, subjects with greater HF-HRV stimulus-evoked response for eRAVANS also demonstrated greater activation in MR. Midbrain raphe nuclei have been shown to modulate the activity of cell groups in the hypothalamus that are in turn involved in autonomic control (Benarroch et al. 1983; Robinson et al. 1985; Petrov et al. 1992; Bell et al. 1999). While this linkage between MR activation and HF-HRV power was found using group level analysis, a more direct linkage will likely require causality analyses on the individual level.

Our brainstem-focused fMRI analysis controlled for multiple factors known to reduce signal in brainstem fMRI data collection and analysis (Sclocco et al. 2018). With regards to data collection, we positioned coronal slices along the longitudinal axis of the brainstem, thereby orienting our slices parallel to the long axis of most brainstem nuclei, including NTS, and parallel to the most prominent axis for cardiorespiratory-induced motion of the brainstem – i.e. cranio-caudal (Terem et al. 2018). In terms of analysis approaches, we collected concurrent cardiac and respiratory data alongside the fMRI data to improve correction of physiological artifacts. Masking brainstem fMRI data prior to smoothing reduced the impact of cardiac pulsation noise from surface brainstem vessels and cerebrospinal fluid from spilling into parenchymal voxels of interest. Also, in computing subjects' evoked fMRI response maps, we used data from a no-stimulation sham control fMRI scan run for which an equivalent duration "event"-related regressor was created with equivalent timing during exhalation or inhalation. This allowed analyses to control for more general respiratory-

linked fMRI signal fluctuation, thereby better isolating the true brainstem response to ABVN stimulation.

Another important point was that stimulation events were of short duration (1 second), thereby avoiding the known high noise regime that hamper fMRI designs using long stimulation blocks, as the power spectrum of BOLD fMRI noise decreases as 1/f with temporal frequency (Zarahn et al. 1997; Birn et al. 2004). Previous taVNS fMRI studies have employed designs with long stimulus durations reflecting clinical parameters, and block lengths up to several minutes (Kraus et al. 2007; Dietrich et al. 2008; Kraus et al. 2013; Frangos et al. 2015; Yakunina et al. 2017; Badran et al. 2018a). Such low task frequency designs might benefit from use of Arterial Spin Labeling fMRI techniques, which exhibit a flat power spectrum (Aguirre et al. 2005; Wang et al. 2011).

Our study also has limitations that should be discussed. For instance, BOLD fMRI signal responses in the brainstem have reduced SNR compared to cortical responses (Sclocco et al. 2018), leading to multiple brainstem fMRI studies using uncorrected thresholds, very low cluster-forming thresholds, or mask-based approaches to restrict the analysis to a smaller volume (Hahn et al. 2013; Kraus et al. 2013; Frangos et al. 2015; Faull et al. 2016; Frangos et al. 2017; Yakunina et al. 2017; Badran et al. 2018a). Nevertheless, the anatomical localization for NTS, NAmb, and SpV in our study was consistent with the known targeting of ABVN and GAN nerve pathways into the medulla as noted by anatomical atlases and previously published results for specific trigeminal nuclei responding to orofacial nociceptive input (Nash et al. 2009; Nash et al. 2010; Youssef et al. 2014). These considerations increased our confidence that the reported activations do not constitute false positive results. Also, while a ROI approach for LC and raphe nuclei response constituted an unbiased framework for comparison, using anatomical ROIs has limitations, as only a subregion of LC and raphe nuclei could have been activated, leading to underestimated effect sizes.

In conclusion, our ultrahigh-field (7T) fMRI study demonstrated that exhalation-gated taVNS enhanced activation in ipsilateral NTS and up-stream monoaminergic source nuclei in the brainstem. eRAVANS also enhanced cardiovagal modulation. These results suggest recruitment of clinically-relevant neurophysiological pathways. Future studies need to explore longer-term physiological effects and explore additional parameters that may influence brain targeting for taVNS stimulation.

Supplementary Material

Refer to Web version on PubMed Central for supplementary material.

Acknowledgements

We thank the following organizations for funding support: US National Institutes for Health (NIH), Office Of The Director (OT2-OD023867); Center for Functional Neuroimaging Technologies (P41-EB015896); National Center for Complementary and Integrative Health (NCCIH), NIH (R61-AT009306, P01-AT006663, R01-AT007550); National Institute of Mental Health (NIMH), NIH (R21-MH103468); National Institute for Arthritis and Musculoskeletal and Skin Diseases (NIAMS), NIH (R01-AR064367); the American Heart Association: (16GRNT26420084). This work also involved the use of instrumentation supported by the NIH Shared

Instrumentation Grant Program and/or High-End Instrumentation Grant Program; specifically, Grant no. S1-0RR023043.

References

Aguirre GK, Detre JA and Wang J (2005). "Perfusion fMRI for functional neuroimaging." Int Rev Neurobiol 66: 213–236. [PubMed: 16387205]

Amatruda TT 3rd, Black DA, McKenna TM, McCarley RW and Hobson JA (1975). "Sleep cycle control and cholinergic mechanisms: differential effects of carbachol injections at pontine brain stem sites." Brain Res 98(3): 501–515. [PubMed: 1182534]

Antonino D, Teixeira AL, Maia-Lopes PM, Souza MC, Sabino-Carvalho JL, Murray AR, Deuchars J and Vianna LC (2017). "Non-invasive vagus nerve stimulation acutely improves spontaneous cardiac baroreflex sensitivity in healthy young men: A randomized placebo-controlled trial." Brain Stimul 10(5): 875–881. [PubMed: 28566194]

Aston-Jones G and Bloom FE (1981). "Norepinephrine-containing locus coeruleus neurons in behaving rats exhibit pronounced responses to non-noxious environmental stimuli." J Neurosci 1(8): 887–900. [PubMed: 7346593]

Aston-Jones G and Cohen JD (2005). "Adaptive gain and the role of the locus coeruleus-norepinephrine system in optimal performance." J Comp Neurol 493(1): 99–110. [PubMed: 16254995]

Avants BB, Tustison NJ, Stauffer M, Song G, Wu B and Gee JC (2014). "The Insight ToolKit image registration framework." Front Neuroinform 8: 44. [PubMed: 24817849]

Badran BW, Dowdle LT, Mithoefer OJ, LaBate NT, Coatsworth J, Brown JC, DeVries WH, Austelle CW, McTeague LM and George MS (2018a). "Neurophysiologic effects of transcutaneous auricular vagus nerve stimulation (taVNS) via electrical stimulation of the tragus: A concurrent taVNS/fMRI study and review." Brain Stimul 11(3): 492–500. [PubMed: 29361441]

Badran BW, Mithoefer OJ, Summer CE, LaBate NT, Glusman CE, Badran AW, DeVries WH, Summers PM, Austelle CW, McTeague LM, Borckardt JJ and George MS (2018b). "Short trains of transcutaneous auricular vagus nerve stimulation (taVNS) have parameter-specific effects on heart rate." Brain Stimul 11(4): 699–708. [PubMed: 29716843]

Baekey DM, Molkov YI, Paton JF, Rybak IA and Dick TE (2010). "Effect of baroreceptor stimulation on the respiratory pattern: insights into respiratory-sympathetic interactions." Respir Physiol Neurobiol 174(1–2): 135–145. [PubMed: 20837166]

Barbieri R, Matten EC, Alabi AA and Brown EN (2005). "A point-process model of human heartbeat intervals: new definitions of heart rate and heart rate variability." American Journal of Physiology. Heart and Circulatory Physiology 288(1): H424–435. [PubMed: 15374824]

Beissner F and Baudrexel S (2014). "Investigating the human brainstem with structural and functional MRI." Frontiers in Human Neuroscience 8: 116. [PubMed: 24616692]

Beliveau V, Svarer C, Frokjaer VG, Knudsen GM, Greve DN and Fisher PM (2015). "Functional connectivity of the dorsal and median raphe nuclei at rest." Neuroimage 116: 187–195. [PubMed: 25963733]

Bell AA, Butz BL and Alper RH (1999). "Cardiovascular responses produced by microinjection of serotonin-receptor agonists into the paraventricular nucleus in conscious rats." J Cardiovasc Pharmacol 33(2): 175–180. [PubMed: 10028923]

Ben-Menachem E, Manon-Espaillat R, Ristanovic R, Wilder B, Stefan H, Mirza W, Tarver W and Wernicke J (1994). "Vagus nerve stimulation for treatment of partial seizures: 1. A controlled study of effect on seizures." Epilepsia 35(3): 616–626. [PubMed: 8026408]

Benarroch EE, Balda MS, Finkielman S and Nahmod VE (1983). "Neurogenic hypertension after depletion of norepinephrine in anterior hypothalamus induced by 6- hydroxydopamine administration into the ventral pons: role of serotonin." Neuropharmacology 22(1): 29–34. [PubMed: 6405300]

Birn RM, Cox RW and Bandettini PA (2004). "Experimental designs and processing strategies for fMRI studies involving overt verbal responses." Neuroimage 23(3): 1046–1058. [PubMed: 15528105]

Brooks JC, Faull OK, Pattinson KT and Jenkinson M (2013). "Physiological noise in brainstem FMRI." Front Hum Neurosci 7: 623. [PubMed: 24109446]

Calabrese E, Hickey P, Hulette C, Zhang J, Parente B, Lad SP and Johnson GA (2015). "Postmortem diffusion MRI of the human brainstem and thalamus for deep brain stimulator electrode localization." Hum Brain Mapp 36(8): 3167–3178. [PubMed: 26043869]

Calhoun VD, Stevens MC, Pearlson GD and Kiehl KA (2004). "fMRI analysis with the general linear model: removal of latency-induced amplitude bias by incorporation of hemodynamic derivative terms." Neuroimage 22(1): 252–257. [PubMed: 15110015]

Camm AJMM, Malik M, Bigger JTGB, Breithardt G, Cerutti S, Cohen R, Coumel P, Fallen E, Kennedy H, Kleiger RE and Lombardi F (1996). "Heart rate variability: standards of measurement, physiological interpretation and clinical use. Task Force of the European Society of Cardiology and the North American Society of Pacing and Electrophysiology." Circulation 93(5): 1043–1065. [PubMed: 8598068]

Chang C, Cunningham JP and Glover GH (2009). "Influence of heart rate on the BOLD signal: the cardiac response function." NeuroImage 44(3): 857–869. [PubMed: 18951982]

Clancy JA, Mary DA, Witte KK, Greenwood JP, Deuchars SA and Deuchars J (2014). "Non-invasive vagus nerve stimulation in healthy humans reduces sympathetic nerve activity." Brain Stimulation 7(6): 871–877. [PubMed: 25164906]

Dergacheva O, Griffioen KJ, Neff RA and Mendelowitz D (2010). "Respiratory modulation of premotor cardiac vagal neurons in the brainstem." Respiratory Physiology & Neurobiology 174(1–2): 102–110. [PubMed: 20452467]

Di Matteo V, Pierucci M, Esposito E, Crescimanno G, Benigno A and Di Giovanni G (2008). "Serotonin modulation of the basal ganglia circuitry: therapeutic implication for Parkinson's disease and other motor disorders." Progress in brain research 172: 423–463. [PubMed: 18772045]

Dietrich S, Smith J, Scherzinger C, Hofmann-Preiss K, Freitag T, Eisenkolb A and Ringler R (2008). "[A novel transcutaneous vagus nerve stimulation leads to brainstem and cerebral activations measured by functional MRI]." Biomed Tech (Berl) 53(3): 104–111. [PubMed: 18601618]

Dorocic IP, Fórth D, Xuan Y, Johansson Y, Pozzi L, Silberberg G, Carlén M and Meletis K (2014). "A whole-brain atlas of inputs to serotonergic neurons of the dorsal and median raphe nuclei." Neuron 83(3): 663–678. [PubMed: 25102561]

Faull OK, Jenkinson M, Ezra M and Pattinson K (2016). "Conditioned respiratory threat in the subdivisions of the human periaqueductal gray." Elife 5.

Fonov V, Evans AC, Botteron K, Almli CR, McKinstry RC, Collins DL and G. Brain Development Cooperative (2011). "Unbiased average age-appropriate atlases for pediatric studies." Neuroimage 54(1): 313–327. [PubMed: 20656036]

Frangos E, Ellrich J and Komisaruk BR (2015). "Non-invasive Access to the Vagus Nerve Central Projections via Electrical Stimulation of the External Ear: fMRI Evidence in Humans." Brain Stimulation 8(3): 624–636. [PubMed: 25573069]

Frangos E and Komisaruk BR (2017). "Access to Vagal Projections via Cutaneous Electrical Stimulation of the Neck: fMRI Evidence in Healthy Humans." Brain Stimul 10(1): 19–27. [PubMed: 28104084]

Garcia RG, Lin RL, Lee J, Kim J, Barbieri R, Sclocco R, Wasan AD, Edwards RR, Rosen BR, Hadjikhani N and Napadow V (2017). "Modulation of brainstem activity and connectivity by respiratory-gated auricular vagal afferent nerve stimulation in migraine patients." Pain 158(8): 1461–1472. [PubMed: 28541256]

Gilbey MP, Jordan D, Richter DW and Spyer KM (1984). "Synaptic mechanisms involved in the inspiratory modulation of vagal cardio-inhibitory neurones in the cat." The Journal of Physiology 356: 65–78. [PubMed: 6520798]

Hahn A, Kranz GS, Seidel E-M, Sladky R, Kraus C, Küblböck M, Pfabigan DM, Hummer A, Grahl A and Ganger S (2013). "Comparing neural response to painful electrical stimulation with functional MRI at 3 and 7 T." Neuroimage 82: 336–343. [PubMed: 23769917]

Handforth A, DeGiorgio CM, Schachter SC, Uthman BM, Naritoku DK, Tecoma ES, Henry TR, Collins SD, Vaughn BV, Gilmartin RC, Labar DR, Morris GL 3rd, Salinsky MC, Osorio I, Ristanovic RK, Labiner DM, Jones JC, Murphy JV, Ney GC and Wheless JW (1998). "Vagus

nerve stimulation therapy for partial-onset seizures: a randomized active-control trial." Neurology 51(1): 48–55. [PubMed: 9674777]

Hein E, Nowak M, Kiess O, Biermann T, Bayerlein K, Kornhuber J and Kraus T (2013). "Auricular transcutaneous electrical nerve stimulation in depressed patients: a randomized controlled pilot study." Journal of Neural Transmission (Vienna, Austria: 1996) 120(5): 821–827.

Jacobs BL and Azmitia EC (1992). "Structure and function of the brain serotonin system." Physiol Rev 72(1): 165–229. [PubMed: 1731370]

Jacobs HI, Wiese S, van de Ven V, Gronenschild EH, Verhey FR and Matthews PM (2015). "Relevance of parahippocampal-locus coeruleus connectivity to memory in early dementia." Neurobiol Aging 36(2): 618–626. [PubMed: 25433457]

Janner H, Klausenitz C, Gurtler N, Hahnenkamp K and Usichenko TI (2018). "Effects of Electrical Transcutaneous Vagus Nerve Stimulation on the Perceived Intensity of Repetitive Painful Heat Stimuli: A Blinded Placebo- and Sham-Controlled Randomized Crossover Investigation." Anesth Analg 126(6): 2085–2092. [PubMed: 29337730]

Keren NI, Lozar CT, Harris KC, Morgan PS and Eckert MA (2009). "In vivo mapping of the human locus coeruleus." Neuroimage 47(4): 1261–1267. [PubMed: 19524044]

Keute M, Ruhnau P and Zaehle T (2018). "Reply to "Reconsidering Sham in Transcutaneous Vagus Nerve Stimulation studies"." Clin Neurophysiol 129(11): 2503–2504. [PubMed: 30249501]

Kiyokawa J, Yamaguchi K, Okada R, Maehara T and Akita K (2014). "Origin, course and distribution of the nerves to the posterosuperior wall of the external acoustic meatus." Anat Sci Int 89(4): 238–245. [PubMed: 24604237]

Kraus T, Hösl K, Kiess O, Schanze A, Kornhuber J and Forster C (2007). "BOLD fMRI deactivation of limbic and temporal brain structures and mood enhancing effect by transcutaneous vagus nerve stimulation." Journal of Neural Transmission (Vienna, Austria: 1996) 114(11): 1485–1493.

Kraus T, Kiess O, Hosl K, Terekhin P, Kornhuber J and Forster C (2013). "CNS BOLD fMRI effects of sham-controlled transcutaneous electrical nerve stimulation in the left outer auditory canal - a pilot study." Brain Stimul 6(5): 798–804. [PubMed: 23453934]

Kreuzer PM, Landgrebe M, Resch M, Husser O, Schecklmann M, Geisreiter F, Poeppl TB, Prasser SJ, Hajak G, Rupprecht R and Langguth B (2014). "Feasibility, safety and efficacy of transcutaneous vagus nerve stimulation in chronic tinnitus: an open pilot study." Brain Stimul 7(5): 740–747. [PubMed: 24996510]

Laqua R, Leutzow B, Wendt M and Usichenko T (2014). "Transcutaneous vagal nerve stimulation may elicit anti-and pro-nociceptive effects under experimentally-induced pain—A crossover placebo-controlled investigation." Autonomic Neuroscience 185: 120–122. [PubMed: 25135040]

Lee HS, Kim M-A, Valentino RJ and Waterhouse BD (2003). "Glutamatergic afferent projections to the dorsal raphe nucleus of the rat." Brain research 963(1): 57–71. [PubMed: 12560111]

Lehtimaki J, Hyvarinen P, Ylikoski M, Bergholm M, Makela JP, Aarnisalo A, Pirvola U, Makitie A and Ylikoski J (2013). "Transcutaneous vagus nerve stimulation in tinnitus: a pilot study." Acta Otolaryngol 133(4): 378–382. [PubMed: 23237096]

Lewis LD, Setsompop K, Rosen BR and Polimeni JR (2018). "Stimulus-dependent hemodynamic response timing across the human subcortical-cortical visual pathway identified through high spatiotemporal resolution 7T fMRI." Neuroimage 181: 279–291. [PubMed: 29935223]

Liu D and Hu Y (1988). "The central projections of the great auricular nerve primary afferent fibers--an HRP transganglionic tracing method." Brain Res 445(2): 205–210. [PubMed: 2453252]

Liu Z, Zhou J, Li Y, Hu F, Lu Y, Ma M, Feng Q, Zhang JE, Wang D, Zeng J, Bao J, Kim JY, Chen ZF, El Mestikawy S and Luo M (2014). "Dorsal raphe neurons signal reward through 5-HT and glutamate." Neuron 81(6): 1360–1374. [PubMed: 24656254]

Loewy AD and Burton H (1978). "Nuclei of the solitary tract: efferent projections to the lower brain stem and spinal cord of the cat." J Comp Neurol 181(2): 421–449. [PubMed: 690272]

Meneses A and Liy-Salmeron G (2012). "Serotonin and emotion, learning and memory." Rev Neurosci 23(5–6): 543–553. [PubMed: 23104855]

Miyazaki M, Arata A, Tanaka I and Ezure K (1998). "Activity of rat pump neurons is modulated with central respiratory rhythm." Neurosci Lett 249(1): 61–64. [PubMed: 9672389]

Miyazaki M, Tanaka I and Ezure K (1999). "Excitatory and inhibitory synaptic inputs shape the discharge pattern of pump neurons of the nucleus tractus solitarii in the rat." Exp Brain Res 129(2): 191–200. [PubMed: 10591893]

Moher Alsady T, Blessing EM and Beissner F (2016). "MICA—A toolbox for masked independent component analysis of fMRI data." Human brain mapping 37(10): 3544–3556. [PubMed: 27168407]

Monti JM (2010). "The structure of the dorsal raphe nucleus and its relevance to the regulation of sleep and wakefulness." Sleep Med Rev 14(5): 307–317. [PubMed: 20153669]

Naidich TP, Duvernoy HM, Delman BN, Sorensen AG, Kollias SS and Haacke EM (2009). Duvernoy's Atlas of the Human Brain Stem and Cerebellum. Vienna, Springer Vienna.

Napadow V, Dhond R, Conti G, Makris N, Brown EN and Barbieri R (2008). "Brain correlates of autonomic modulation: combining heart rate variability with fMRI." Neuroimage 42(1): 169–177. [PubMed: 18524629]

Napadow V, Dhond R, Kennedy D, Hui KK and Makris N (2006). "Automated brainstem co-registration (ABC) for MRI." Neuroimage 32(3): 1113–1119. [PubMed: 16839781]

Napadow V, Edwards RR, Cahalan CM, Mensing G, Greenbaum S, Valovska A, Li A, Kim J, Maeda Y, Park K and Wasan AD (2012). "Evoked pain analgesia in chronic pelvic pain patients using respiratory-gated auricular vagal afferent nerve stimulation." Pain Medicine (Malden, Mass.) 13(6): 777–789.

Nash PG, Macefield VG, Klineberg IJ, Gustin SM, Murray GM and Henderson LA (2010). "Bilateral activation of the trigeminothalamic tract by acute orofacial cutaneous and muscle pain in humans." Pain 151(2): 384–393. [PubMed: 20732744]

Nash PG, Macefield VG, Klineberg IJ, Murray GM and Henderson LA (2009). "Differential activation of the human trigeminal nuclear complex by noxious and non-noxious orofacial stimulation." Hum Brain Mapp 30(11): 3772–3782. [PubMed: 19492300]

Neff RA, Wang J, Baxi S, Evans C and Mendelowitz D (2003). "Respiratory sinus arrhythmia: endogenous activation of nicotinic receptors mediates respiratory modulation of brainstem cardioinhibitory parasympathetic neurons." Circulation Research 93(6): 565–572. [PubMed: 12907666]

Nemeroff CB, Mayberg HS, Krahl SE, McNamara J, Frazer A, Henry TR, George MS, Charney DS and Brannan SK (2006). "VNS therapy in treatment-resistant depression: clinical evidence and putative neurobiological mechanisms." Neuropsychopharmacology 31(7): 1345–1355. [PubMed: 16641939]

Nomura S and Mizuno N (1984). "Central distribution of primary afferent fibers in the Arnold's nerve (the auricular branch of the vagus nerve): a transganglionic HRP study in the cat." Brain Research 292(2): 199–205. [PubMed: 6692153]

Norgren R (1978). "Projections from the nucleus of the solitary tract in the rat." Neuroscience 3(2): 207–218. [PubMed: 733004]

Olszewski J and Baxter D (1954). "Cytoarchitecture of the human brain stem." Cytoarchitecture of the human brain stem.

Petrov T, Krukoff TL and Jhamandas JH (1992). "The hypothalamic paraventricular and lateral parabrachial nuclei receive collaterals from raphe nucleus neurons: a combined double retrograde and immunocytochemical study." J Comp Neurol 318(1): 18–26. [PubMed: 1583154]

Piepoli M, Sleight P, Leuzzi S, Valle F, Spadacini G, Passino C, Johnston J and Bernardi L (1997). "Origin of respiratory sinus arrhythmia in conscious humans. An important role for arterial carotid baroreceptors." Circulation 95(7): 1813–1821. [PubMed: 9107168]

Polimeni JR, Bhat H, Witzel T, Benner T, Feiweier T, Inati SJ, Renvall V, Heberlein K and Wald LL (2016). "Reducing sensitivity losses due to respiration and motion in accelerated echo planar imaging by reordering the autocalibration data acquisition." Magn Reson Med 75(2): 665–679. [PubMed: 25809559]

Rangon CM (2018). "Reconsidering Sham in Transcutaneous Vagus Nerve Stimulation studies." Clin Neurophysiol 129(11): 2501–2502. [PubMed: 30268709]

Robinson SE, Austin MJ and Gibbens DM (1985). "The role of serotonergic neurons in dorsal raphe, median raphe and anterior hypothalamic pressor mechanisms." Neuropharmacology 24(1): 51–58. [PubMed: 3982602]

Rong P-J, Fang J-L, Wang L-P, Meng H, Liu J, Ma Y.-g., Ben H, Li L, Liu R-P and Huang Z-X (2012). "Transcutaneous vagus nerve stimulation for the treatment of depression: a study protocol for a double blinded randomized clinical trial." BMC Complementary and Alternative Medicine 12(1): 255. [PubMed: 23241431]

Sackeim HA, Rush AJ, George MS, Marangell LB, Husain MM, Nahas Z, Johnson CR, Seidman S, Giller C, Haines S, Simpson RK Jr. and Goodman RR (2001). "Vagus nerve stimulation (VNS) for treatment-resistant depression: efficacy, side effects, and predictors of outcome." Neuropsychopharmacology 25(5): 713–728. [PubMed: 11682255]

Saper CB and Loewy AD (1980). "Efferent connections of the parabrachial nucleus in the rat." Brain Res 197(2): 291–317. [PubMed: 7407557]

Saper CB and Stornetta RL (2015). Central autonomic system The Rat Nervous System (Fourth Edition), Elsevier: 629–673.

Sara SJ (2009). "The locus coeruleus and noradrenergic modulation of cognition." Nat Rev Neurosci 10(3): 211–223. [PubMed: 19190638]

Schreihofer AM and Guyenet PG (2003). "Baro-activated neurons with pulse-modulated activity in the rat caudal ventrolateral medulla express GAD67 mRNA." Journal of Neurophysiology 89(3): 1265–1277. [PubMed: 12612005]

Sclocco R, Beissner F, Bianciardi M, Polimeni JR and Napadow V (2018). "Challenges and opportunities for brainstem neuroimaging with ultrahigh field MRI." Neuroimage 168: 412–426. [PubMed: 28232189]

Sclocco R, Beissner F, Desbordes G, Polimeni JR, Wald LL, Kettner NW, Kim J, Garcia RG, Renvall V, Bianchi AM, Cerutti S, Napadow V and Barbieri R (2016). "Neuroimaging brainstem circuitry supporting cardiovagal response to pain: a combined heart rate variability/ultrahigh-field (7 T) functional magnetic resonance imaging study." Philos Trans A Math Phys Eng Sci 374(2067).

Sclocco R, Kim J, Garcia RG, Sheehan JD, Beissner F, Bianchi AM, Cerutti S, Kuo B, Barbieri R and Napadow V (2014). "Brain Circuitry Supporting Multi-Organ Autonomic Outflow in Response to Nausea." Cerebral Cortex (New York, N.Y.: 1991).

Spyer KM (1981). "Neural organisation and control of the baroreceptor reflex." Reviews of Physiology, Biochemistry and Pharmacology 88: 24–124.

Straube A, Ellrich J, Eren O, Blum B and Ruscheweyh R (2015). "Treatment of chronic migraine with transcutaneous stimulation of the auricular branch of the vagal nerve (auricular t- VNS): a randomized, monocentric clinical trial." J Headache Pain 16: 543. [PubMed: 26156114]

Terem I, Ni WW, Goubran M, Rahimi MS, Zaharchuk G, Yeom KW, Moseley ME, Kurt M and Holdsworth SJ (2018). "Revealing sub-voxel motions of brain tissue using phase- based amplified MRI (aMRI)." Magn Reson Med.

Usichenko T, Laqua R, Leutzow B and Lotze M (2017). "Preliminary findings of cerebral responses on transcutaneous vagal nerve stimulation on experimental heat pain." Brain Imaging Behav 11(1): 30–37. [PubMed: 26781484]

Van Bockstaele EJ, Peoples J and Telegan P (1999). "Efferent projections of the nucleus of the solitary tract to peri-locus coeruleus dendrites in rat brain: Evidence for a monosynaptic pathway." Journal of Comparative Neurology 412(3): 410–428. [PubMed: 10441230]

Ventureyra EC (2000). "Transcutaneous vagus nerve stimulation for partial onset seizure therapy. A new concept." Child's Nervous System: ChNS: Official Journal of the International Society for Pediatric Neurosurgery 16(2): 101–102.

Vertes RP and Linley SB (2008). Efferent and afferent connections of the dorsal and median raphe nuclei in the rat Serotonin and sleep: molecular, functional and clinical aspects, Springer: 69–102.

Wang DJ, Chen Y, Fernandez-Seara MA and Detre JA (2011). "Potentials and challenges for arterial spin labeling in pharmacological magnetic resonance imaging." J Pharmacol Exp Ther 337(2): 359–366. [PubMed: 21317356]

Wang QP and Nakai Y (1994). "The dorsal raphe: an important nucleus in pain modulation." Brain Res Bull 34(6): 575–585. [PubMed: 7922601]

Wehrwein EA and Joyner MJ (2013). "Regulation of blood pressure by the arterial baroreflex and autonomic nervous system." Handbook of Clinical Neurology 117: 89–102. [PubMed: 24095118]

Yakunina N, Kim SS and Nam EC (2017). "Optimization of Transcutaneous Vagus Nerve Stimulation Using Functional MRI." Neuromodulation 20(3): 290–300. [PubMed: 27898202]

Ylikoski J, Lehtimaki J, Pirvola U, Makitie A, Aarnisalo A, Hyvarinen P and Ylikoski M (2017). "Non-invasive vagus nerve stimulation reduces sympathetic preponderance in patients with tinnitus." Acta Otolaryngol 137(4): 426–431. [PubMed: 28084177]

Youssef AM, Gustin SM, Nash PG, Reeves JM, Petersen ET, Peck CC, Murray GM and Henderson LA (2014). "Differential brain activity in subjects with painful trigeminal neuropathy and painful temporomandibular disorder." Pain 155(3): 467–475. [PubMed: 24269492]

Yuan H and Silberstein SD (2015). "Vagus Nerve and Vagus Nerve Stimulation, a Comprehensive Review: Part IN." Headache.

Zarahn E, Aguirre GK and D'Esposito M (1997). "Empirical analyses of BOLD fMRI statistics. I. Spatially unsmoothed data collected under null-hypothesis conditions." Neuroimage 5(3): 179–197. [PubMed: 9345548]

Zoccal DB, Furuya WI, Bassi M, Colombari DS and Colombari E (2014). "The nucleus of the solitary tract and the coordination of respiratory and sympathetic activities." Front Physiol 5: 238. [PubMed: 25009507]

Highlights

- Respiration influences the activity of NTS, which is facilitated during exhalation.
- The effects of auricular vagus nerve stimulation can be optimized with respiratory gating.
- We use 7T fMRI and heart rate variability to investigate central and peripheral responses to tVNS.
- Exhalation-gated tVNS enhances engagement of key neuromodulator brainstem nuclei.
- Exhalation-gated tVNS increases stimulus-evoked cardiovagal outflow.

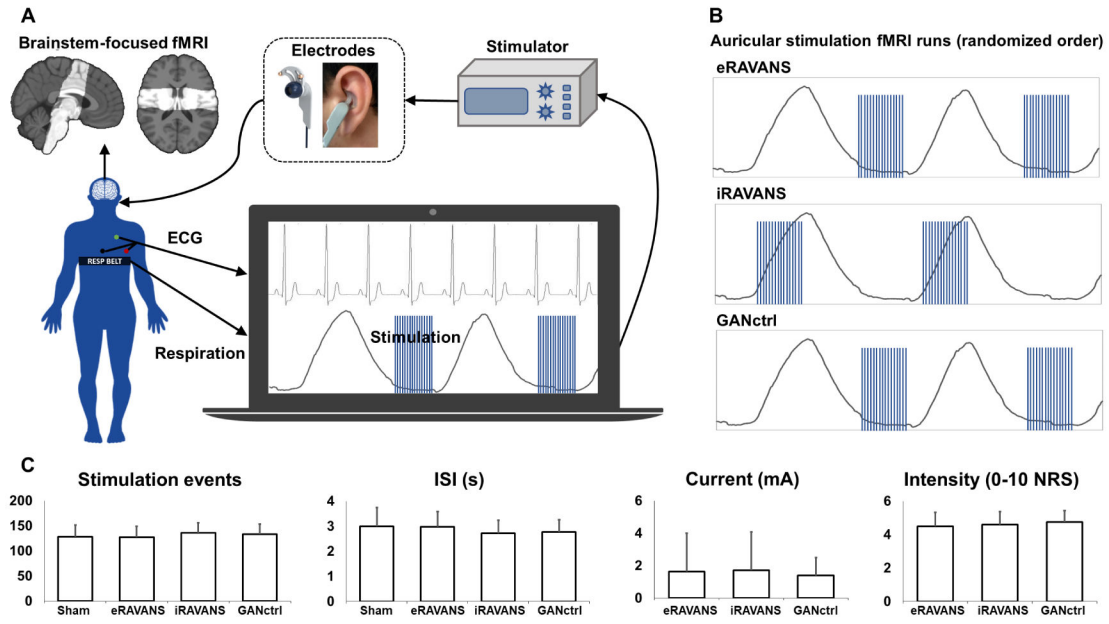

Figure 1 –.

(A) Experimental setup for data collection: fMRI data were collected with partial brain coverage focused on the brainstem (group-consistent coverage shown). Concurrently to fMRI, electrocardiography (ECG) and respiration signals were monitored, and the latter was used to trigger in real-time the onset of respiration-gated left auricular stimulation, delivered through custom electrodes placed either in the cymba conchae (RAVANS taVNS runs) or over the earlobe (greater auricular nerve control, GANctrl). (B) Example respiratory traces showing timing for exhalation-gated RAVANS (eRAVANS), inhalation-gated RAVANS (iRAVANS), and exhalation-gated GANctrl stimulation, counterbalanced across subjects. (C) Stimulation parameters (number of events, inter-stimulus interval (ISI), current) and ratings were not significantly different across conditions. Error bars represent SD.

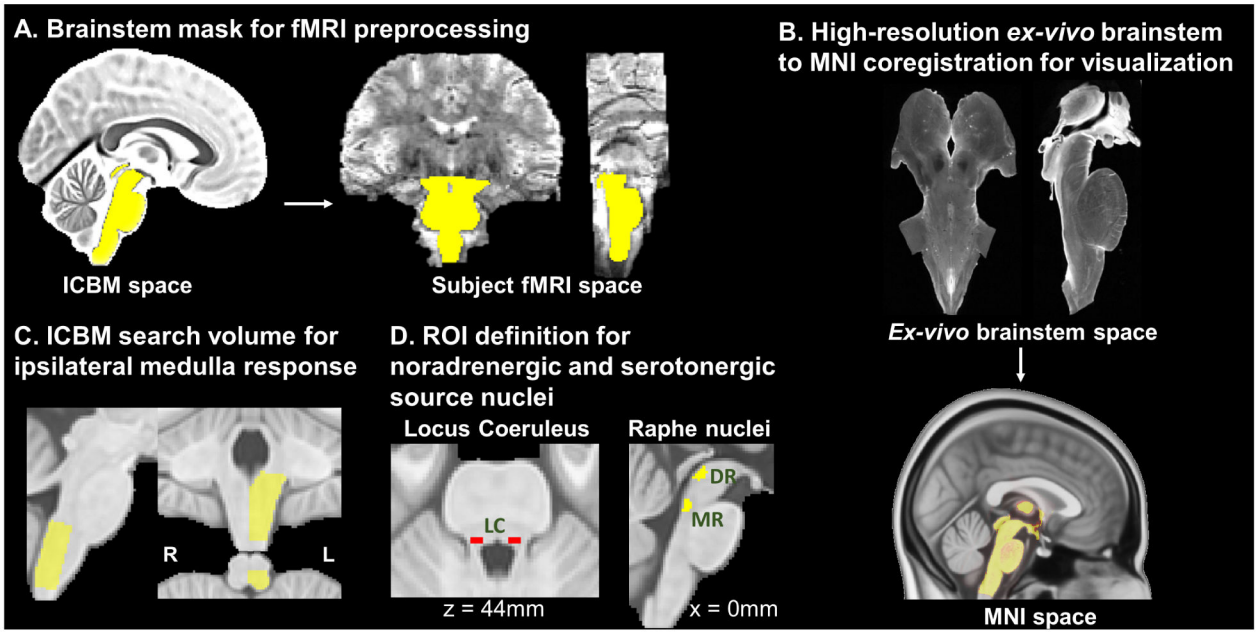

Figure 2 –.

(A) A brainstem mask defined in ICBM space was transformed to subjects' individual fMRI space and used to retain brainstem voxels and mitigate physiological noise contamination introduced by spatial smoothing. (B) A high-resolution (0.2 mm isotropic voxels) *ex vivo* brainstem volume (courtesy of Calabrese et al. 2015) was transformed to MNI space; transformation matrices were inverted and applied to the final group fMRI maps to aid visualization and comparison with brainstem atlases. (C) A volume including the left (ipsilateral to stimulation side) dorsal medulla was defined in ICBM space and used as a search space for evaluation of dorsal medullary brainstem responses to RAVANS and GANctrl stimulation runs. (D) ROIs for noradrenergic (LC; (Keren et al. 2009)) and serotonergic (DR, MR; (Beliveau et al. 2015)) nuclei were defined based on results of previous neuroimaging studies.

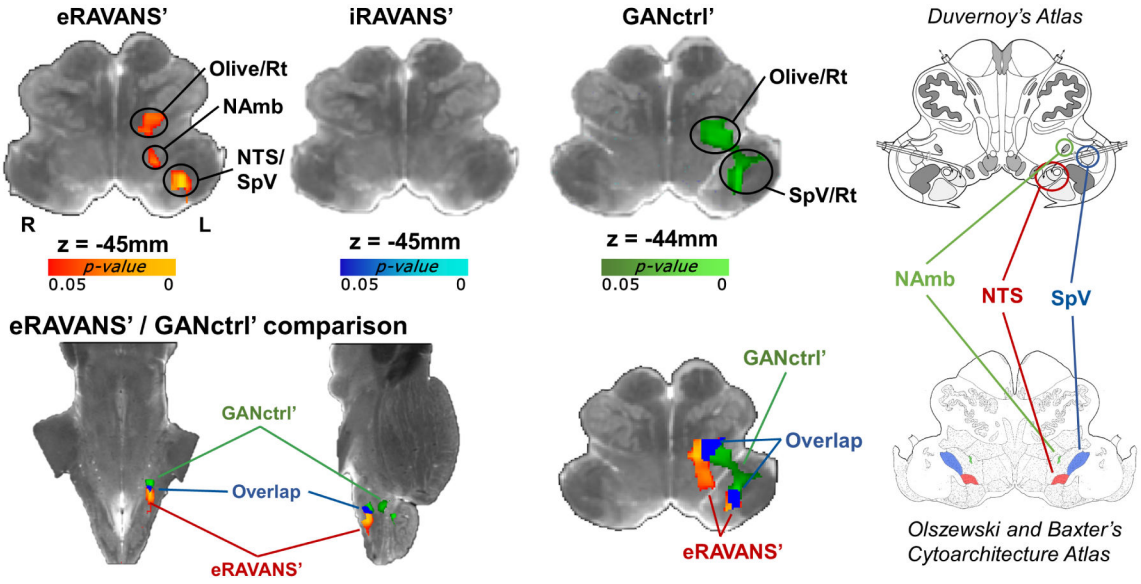

Figure 3 –.

Top row: group maps showing masked ipsilateral medullary responses to exhalatory taVNS (eRAVANS'), inhalatory taVNS (iRAVANS') and greater auricular nerve control stimulation over the earlobe (GANctrl'), overlaid on a high-resolution (0.2 mm) *ex vivo* brainstem. The respiration phase-matched sham (eSham, iSham) was subtracted from each active stimulation condition in order to normalize active stimulation response and control for respiratory modulation of the fMRI signal. Bottom row: eRAVANS' (red-yellow) and GANctrl' (green) group maps, as well as their overlap (blue), are shown on the same underlay. The corresponding brainstem slices from the Duvernoy's (top right) and the Olszewski and Baxter's (bottom right) atlases aid the localization of functional responses. The eRAVANS' cluster is consistent with purported NAmb, NTS and part of SpV, whereas the GANctrl' response mainly involves a cluster more consistent with SpV.

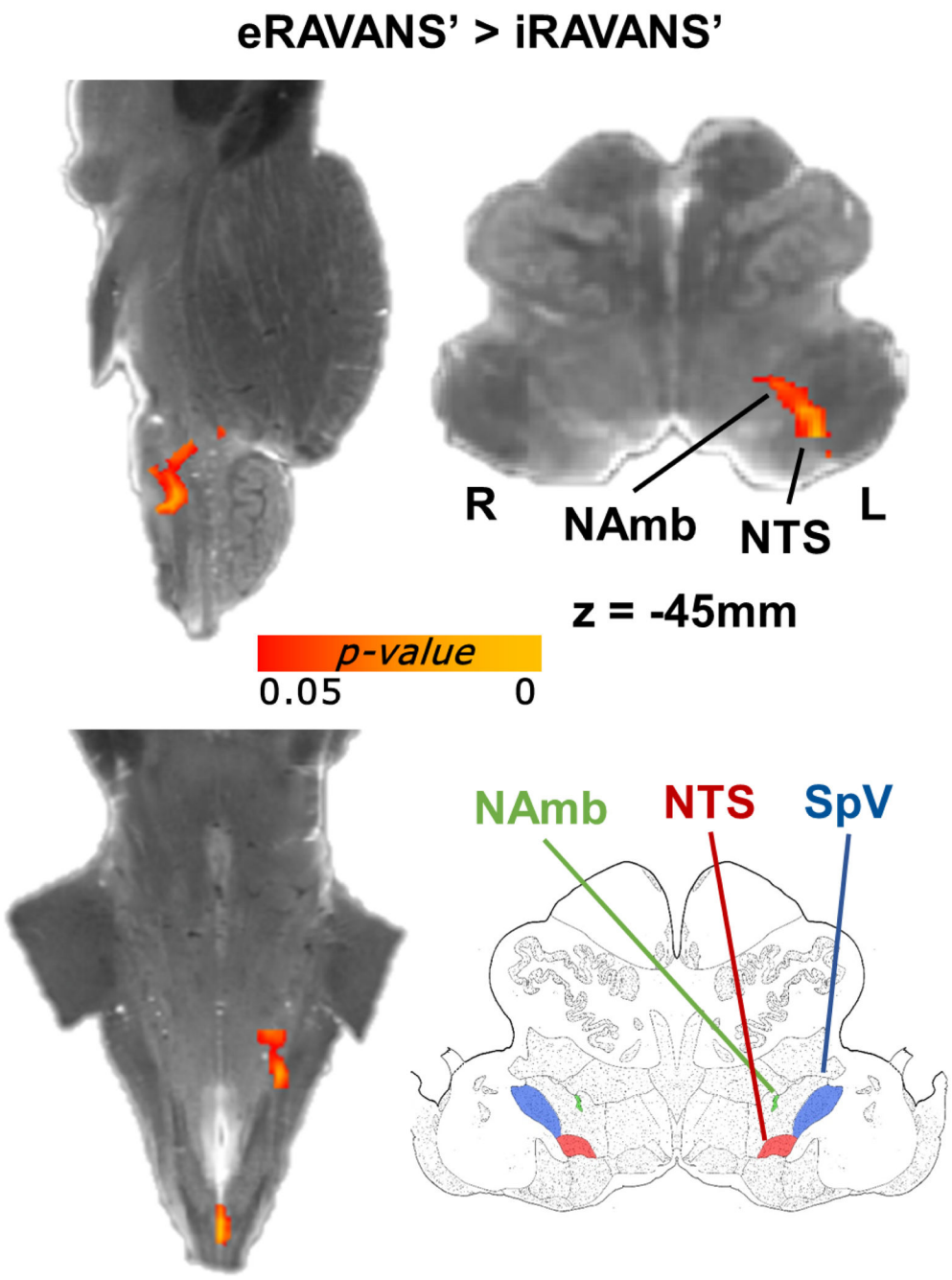

Figure 4 –.

Direct comparison between eRAVANS' and iRAVANS' responses noted greater NTS and NAmb activation for eRAVANS'.

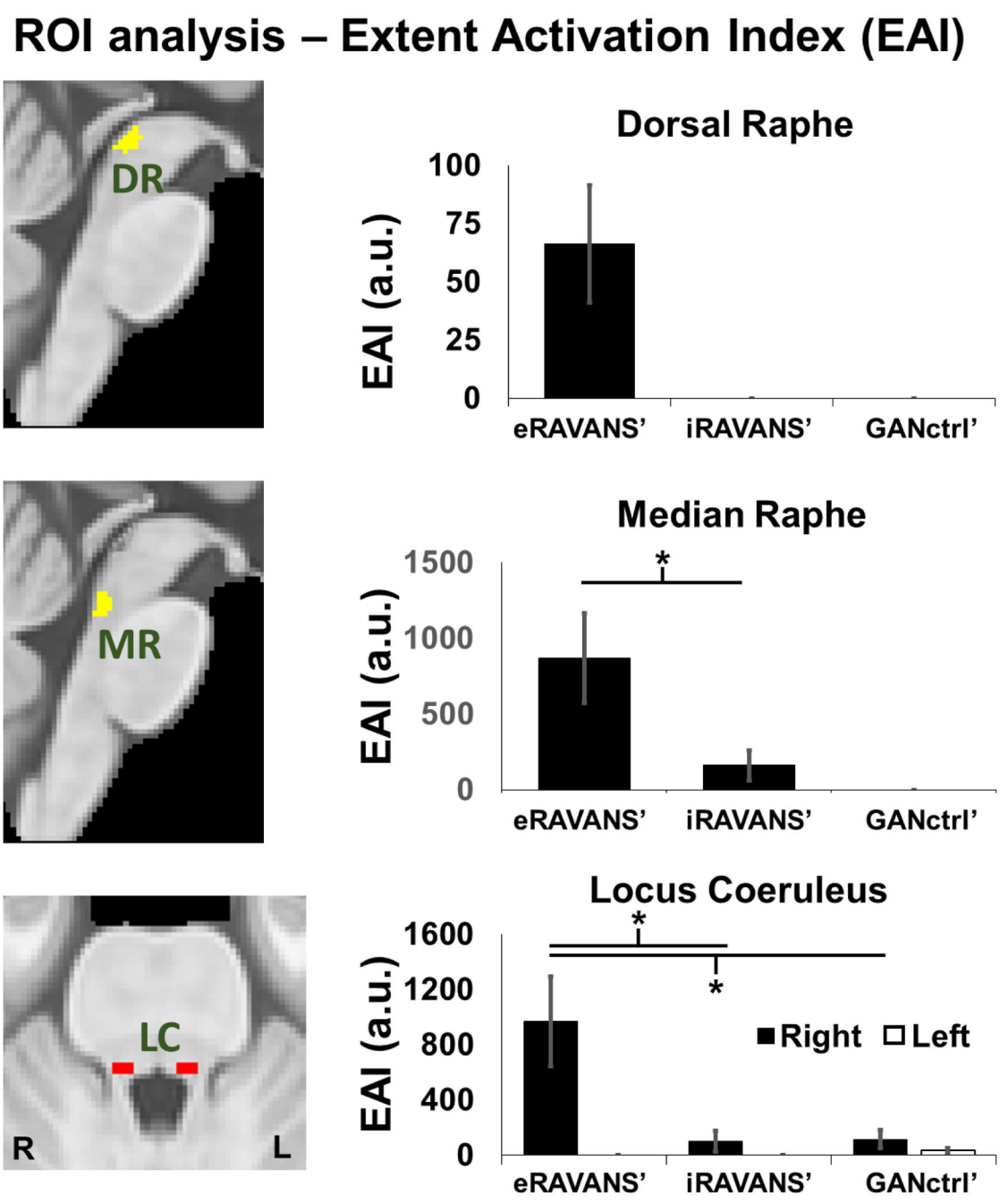

Figure 5 –.

ROI analysis found that eRAVANS' produced greater response than both iRAVANS' and GANctrl' in serotonergic (DR, MR) and noradrenergic (LC) source brainstem nuclei. Analyses use an Extent Activation Index (EAI), which weighted the activation strength by its extent within the ROI volume. * = $p < 0.05$; error bars show SEM.

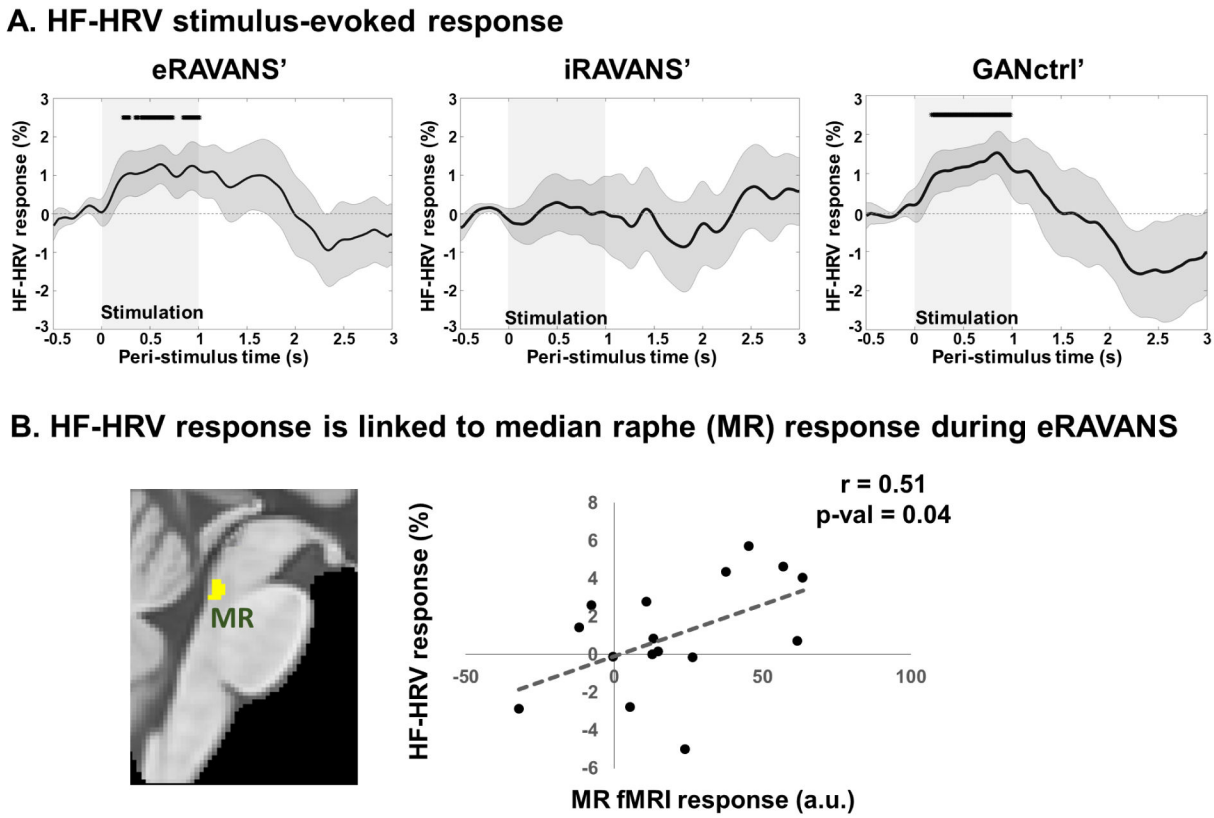

Figure 6 –.

(A) Stimulus-evoked HF-HRV power response to stimulation. eRAVANS' panel: * = eRAVANS > eSham, $p < 0.05$. GANctrl' panel: * = GANctrl > eSham, $p < 0.05$. (B) Subjects' stimulus-evoked HF-HRV response (0-2 s post-stimulation) was correlated with fMRI response in the MR nucleus (basis function summary statistic).

Table I –

Stimulation characteristics and subjects' ratings for the different conditions (mean ± SD; ISI: inter-stimulus interval).

Condition	# stimuli	ISI (s)	Current (mA)	Intensity (0-10 NRS)
eSham / iSham	127.9 ± 23.8	3.0 ± 0.7	-	-
eRAVANS	127.5 ± 22.0	2.9 ± 0.6	1.6 ± 2.3	4.5 ± 0.8
iRAVANS	136.1 ± 20.3	2.7 ± 0.5	1.7 ± 2.4	4.6 ± 0.8
GANctrl	133.8 ± 19.8	2.8 ± 0.5	1.4 ± 1.1	4.7 ± 0.7